Journal of Materials Chemistry A

RSC Publishing

COMMUNICATION

View Article Online
View Journal | View Issue

Enhanced rate capabilities of Co_3O_4/carbon nanotube anodes for lithium ion battery applications

Cite this: *J. Mater. Chem. A*, 2013, **1**, 11121

Received 4th July 2013
Accepted 24th July 2013

DOI: 10.1039/c3ta12608k

www.rsc.org/MaterialsA

Xingfeng He, Yang Wu, Fei Zhao, Jiaping Wang,* Kaili Jiang and Shoushan Fan

Co_3O_4 nanoparticles with a mass loading over 70 wt% are homogeneously grown on super-aligned carbon nanotube films using a pyrolysis method with $Co(NO_3)_2$ as a precursor. Benefiting from the flexible and highly conductive carbon nanotube scaffold, the Co_3O_4/carbon nanotube composite electrode exhibits great cycling stability (910 mA h g^{-1} after 50 cycles at 0.1 C) as well as excellent rate performance (820 mA h g^{-1} at 1 C), and can be considered as a promising anode material for high performance lithium ion batteries.

Lithium-ion batteries (LIBs) have been widely expected to be an energy storage solution for the next-generation electric vehicles. To this end, one of the restrictions to the practical application of LIBs as power cells for the electrical vehicles (EVs) is their low energy densities and power densities.[1–4] Accordingly, great efforts have been dedicated to seek potential electrode materials in place of commercial $LiCoO_2$ and graphite with higher lithium storage capacity and, particularly, greater power density. During the last decade, transition metal oxides were identified as a new class of anode materials.[5–17] In comparison with the insertion mechanism in graphite, transition metal oxides were reduced to elementary metals that were embedded into the Li_2O matrix in the lithiation process *via* a conversion reaction mechanism.[9,18] As a result, the theoretical capacity of a transition metal oxide is directly related to the number of oxygen atoms per chemical formula. For instance, Co_3O_4 exhibits a theoretical capacity of 890 mA h g^{-1}, according to the conversion reaction, which is remarkably higher than that of graphite (372 mA h g^{-1} with an end compound of LiC_6).[19] Even though Co_3O_4 possesses such a high lithium storage capacity, it suffered from a number of problems such as short cycle life, fast capacity fading, and poor capacities delivered at high rates, which often occurred in transition-metal oxides.[6,7,11,14] These problems can be attributed to their low electric and ionic conductivity. Decreasing the particle size turned out to be effective in shortening the lithium ion diffusion length in the active material. Indeed, the first lithiation/delithiation cycle always coincided with a significant morphology change in Co_3O_4.[10,20] Thus, lithium storage *via* a conversion reaction was unambiguously associated with a high kinetic barrier and only available in nano-scaled materials.

Although the size of the active material was an important variable to alter the mass transfer, it made less contribution with respect to the electrical conductivity. The strategy has been shifted to the introduction of conductive additives compatible with the active electrode material in dimensions to enhance the electron transfer efficiency and to improve the performance at high rates. For instance, hybrid gold–cobalt oxide nanowires were fabricated to facilitate electron transport.[7] The same idea has been manifested by coating Fe_3O_4 nanoparticles on Cu nano-pillars electrochemically.[14] The problem is the requirement of the precise control of experimental conditions and the heavy mass introduced by the Cu nano-pillars. Accordingly, lightweight and conductive carbon additives were extensively explored.[6–9,11,12,21–24] For example, graphene or graphene nanoribbons were used to wrap Co_3O_4, MnO_2, and SnO_2nanoparticles, forming a good conductive coating.[6,12,25] These composite electrodes showed both promising reversible capacities and capacity retention. However, in such composites, conductive carbon blacks such as acetylene black and complex experimental procedures were still required. Another barrier to their practical application is that the production is only available at the lab-scale.

Following the similar idea of making a compatible conductive additive and current collector for each active particle, we identify that carbon nanotubes (CNTs) would be a promising material.[26,27] General fabrication methods of CNT-based composite electrodes involve the direct deposition of active material onto CNTs. In contrast to carbon coating or wrapping, the most significant advantage of using CNTs as conductive additives and current collectors is the exposure of the majority of the active particles to the electrolyte, suggesting little sacrifice in lithium ion transfer. Among all types of CNTs, the super-aligned CNT (SACNT) is remarkable due to its large aspect ratio,

Department of Physics and Tsinghua-Foxconn Nanotechnology Research Center, Tsinghua University, Beijing 100084, P. R. China. E-mail: jpwang@tsinghua.edu.cn

high degree of graphitization, and little amorphous carbon deposition on the surface. In the past, it has been demonstrated that SACNTs could be used as current collectors for LIBs[28] or as conductive additives to significantly improve both reversible capacity and capacity retention of SnO_2.[29] The fabrication of SnO_2/SACNT composites involved a multiple-step procedure with necessary linking agents and presented a low loading of SnO_2 (63 wt%). Such drawbacks made the SnO_2/SACNT material system far from large-scale applications.

Herein, we report a facile and scalable fabrication method for high rate Co_3O_4/SACNT composite anodes for LIBs. In contrast to SnO_2, Co_3O_4 will not involve the lithium alloying procedure. Therefore, this material system will not present huge volumetric change, which is more ideal for practical applications. Co_3O_4 nanoparticles are synthesized by the pyrolysis of $Co(NO_3)_2$ (Fig. 1). SACNTs are first assembled into continuous CNT films from SACNT arrays. This step affords a flexible and highly conductive SACNT scaffold to host Co_3O_4 particles. In this method, the electrodes contain over 70 wt% Co_3O_4 as active material and SACNTs as the structural framework, conductive additive, and current collector. The Co_3O_4/SACNT composite anodes exhibit high electrical conductivity, great mechanical properties, high energy density, and specifically outstanding rate capability (820 mA h g^{-1} at 1 C) based on the mass of the Co_3O_4/SACNT. Since the SACNT films have been mass produced with a high number of applications,[30] we may expect that this easy process would have great promise for high power LIB applications beyond lab scales.

Fig. 1 illustrates the synthesis procedure for making Co_3O_4/SACNT composite anodes. SACNT arrays consisting of CNTs with a diameter of 20–30 nm and a height of 300 μm were synthesized on 4 inch silicon wafers by chemical vapor deposition. Details of the synthesis procedure can be found in previous papers.[27,31–33] A continuous SACNT film was drawn from SACNT arrays and 100 layers of SACNT films were cross-stacked onto a polytetrafluoroethylene (PTFE) frame using a lab-designed apparatus. $Co(NO_3)_2$ solution was prepared by mixing 1 M $Co(NO_3)_2$ aqueous solution and isopropanol at a volume ratio of 4 : 1. After soaking the SACNT film together with the PTFE frame in the $Co(NO_3)_2$ solution for 2 days, the obtained $Co(NO_3)_2$/SACNT composite precursor was calcined at 300 °C in a nitrogen flow for 1 h. Nano-sized cobalt oxide particles were easily accessed *via* the pyrolysis of $Co(NO_3)_2$, leading to the formation of the cobalt oxide/SACNT composite.

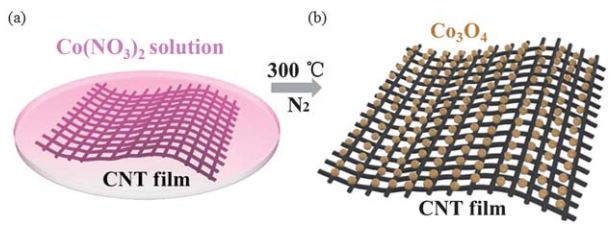

Fig. 1 The schematic illustration of the synthesis of a Co_3O_4/SACNT composite electrode. (a) A cross-stacked SACNT film soaked in $Co(NO_3)_2$ solution; (b) nano-sized Co_3O_4 particles *in situ* grown on the SACNT film *via* the pyrolysis of $Co(NO_3)_2$.

Fig. 2a shows an SEM image of the top view of an as-prepared SACNT film containing 100 CNT layers. After the *in situ* growth of cobalt oxide nanoparticles on SACNTs, the porous and ordered structure of the SACNT film was largely retained (Fig. 2b). SEM and TEM studies revealed no obvious aggregated cobalt oxide nanoparticles, as shown in Fig. 2b and c. The product was confirmed to be Co_3O_4 by XRD. The XRD pattern in Fig. 2d clearly showed that the diffraction peaks of the specimen agree well with those of crystalline Co_3O_4 [space group: *Fd3m* (227)].[6] The additional diffraction peak near 26° can be indexed to the (002) reflection of CNTs. The pyrolysis of $Co(NO_3)_2$ successfully afforded Co_3O_4 nanoparticles that were anchored homogeneously on the SACNT film without any prior functionalization steps. It is worth noting that this fabrication procedure of composite electrodes is binder-free, suggesting great potential in enhancing the energy density. According to the mass of the SACNT films and the Co_3O_4/SACNT composite, the weight percentages of Co_3O_4 can be calculated. The final loadings of the oxides on the SACNT films can be adjusted by the concentration of the

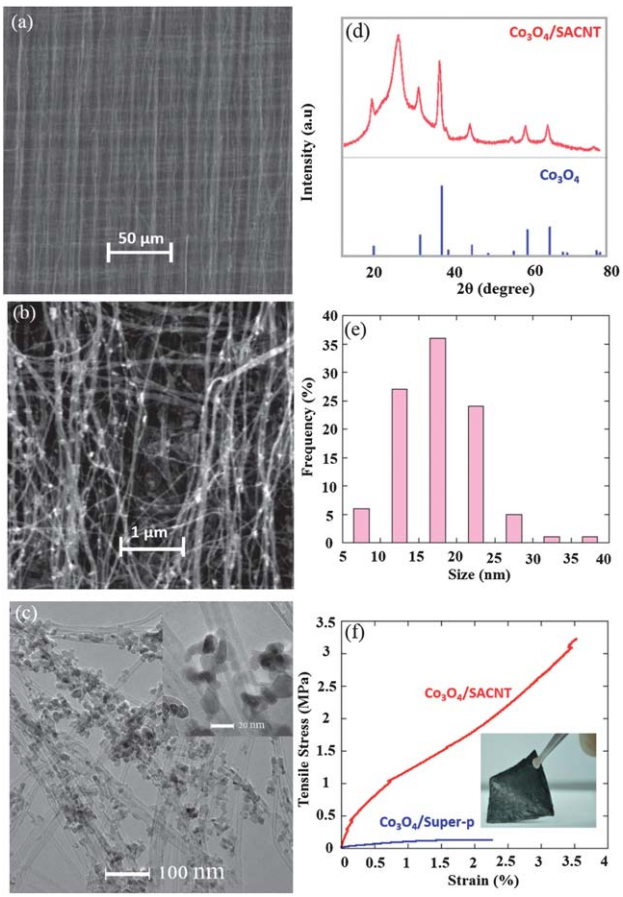

Fig. 2 SEM images of (a) a pristine SACNT film and (b) a Co_3O_4/SACNT composite electrode; (c) TEM images of a Co_3O_4/SACNT composite electrode in low and high magnifications; (d) XRD pattern of a Co_3O_4/SACNT composite. Blue lines are calculated peak positions according to the crystal structure information of Co_3O_4; (e) size distribution of Co_3O_4 nanoparticles according to the TEM images; (f) stress–strain curves of the Co_3O_4/SACNT and Co_3O_4/Super-P composites and photograph of a flexible Co_3O_4/SACNT composite (inset).

$Co(NO_3)_2$ solutions. Two typical samples possessing 77 wt% and 72 wt% of Co_3O_4 are presented in this paper. The mass loadings of Co_3O_4 are determined by measuring the weight of the original CNT film and the obtained Co_3O_4/CNT composite, which agree well with those measured by thermogravimetric analysis (TGA).

The SACNT film also regulated the growth of Co_3O_4 nanoparticles. The particle size of Co_3O_4 was analyzed with the TEM study, which suggested a size distribution of 10–25 nm (Fig. 2e). As illustrated in the TEM images (Fig. 2c), almost all the Co_3O_4 nanoparticles were anchored on the sidewall of CNTs. The intimate contact between Co_3O_4 and CNTs avoided aggregation of Co_3O_4 nanoparticles. We attribute this homogeneous *in situ* synthesis of Co_3O_4 nanoparticles on CNTs to the template effect of the SACNT film. The small pores inside the SACNT film may regulate the growth and confine the size of the Co_3O_4 nanoparticles. The intact network structure composed of aligned CNTs ensures uniform anchoring of Co_3O_4 nanoparticles on the conductive CNT pathways throughout the electrode. Additionally, we did not observe any structural destruction on individual CNTs in high-resolution TEM images. Therefore, we may conclude that the electrical property of CNTs is well preserved, which will greatly benefit the electrical conductivity of the composite electrode.

Indeed, the conductivity of the electrode plays a critical role in power cells. The high internal resistance will result in polarization and fast capacity fading, particularly in high power applications. The excess of Joule heat associated with high internal resistance will also cause safety concerns. However, the continuous SACNT film improves the conductivity of the electrode significantly. As a result, the Co_3O_4/SACNT composite (containing 77 wt% Co_3O_4) exhibited a resistivity of as low as 1.6×10^{-4} Ω m. In order to demonstrate the superiority of the Co_3O_4/SACNT composite, the Co_3O_4/Super-P composite (containing 80 wt% commercial Co_3O_4 with a diameter of 10–30 nm) as a control sample was prepared with a traditional slurry cast method. Such samples showed a resistivity of 4.6×10^{-2} Ω m, which is two orders of magnitude higher than that of the Co_3O_4/SACNT composite. This difference proved the above advantage of the utilization of the ordered network structure of SACNTs in the composite electrode.

Another important factor that should be taken into account is the mechanical stability of the electrode. Generally, low strength of the electrodes will result in cracks or voids in the electrodes, because of the variation in volume during the charge–discharge processes. The overall mechanical strength of the composite electrode can be greatly benefited from SACNTs. According to the stress–strain curves, the Co_3O_4/SACNT composite showed a higher strength and was more flexible than the Co_3O_4/Super-P composite (Fig. 2f). The Young's modulus, tensile strength, and strain at fracture of the Co_3O_4/SACNT specimen were 160 MPa, 3.5 MPa, and 3.2%, respectively. For comparison, these values are 6.4 times, 27.2 times, and 1.6 times those of the Co_3O_4/super-P specimen, respectively. Both the higher flexibility and strength of the Co_3O_4/SACNT composite are indicative of better endurance of the volume change during charge–discharge cycles.

Coin-type half-cells were assembled with the Co_3O_4/SACNT composite, Co_3O_4/Super-P composite, and CNT films as the positive electrode and Li metal as the negative electrode. The electrochemical performance of the 77 wt% Co_3O_4/SACNT composite electrodes was investigated at 0.1 C rate in the potential range from 0.01 V to 3 V at room temperature (Fig. 3a and b). The capacity values are calculated based on the mass of the Co_3O_4/SACNT electrode. The voltage–capacity curve of the Co_3O_4/SACNT electrode featured a long voltage plateau at about 1.1 V and sloped down to the cut-off voltage of 0.01 V during the first discharge step, which agrees well with a previous study.[10] According to the investigations by Tarascon, this voltage plateau was related to an intermediate phase of lithium intercalation ($Li_xCo_3O_4$) and then a full reduction to form Co and Li_2O.[34] The discharge and charge capacities for the first cycle were 1200 and 815 mA h g^{-1} for the Co_3O_4/SACNT composite. The high discharge capacity for the first cycle compared to its theoretical capacity of 890 mA h g^{-1} may be attributed to the formation of a partially irreversible solid electrolyte interface (SEI) film.[10] The slight increase in the capacity of the Co_3O_4/SACNT composite during the first 20 cycles may result from the large effective surface, which would offer extra adsorption sites for Li ions. At the 20th cycle, the specific capacity rose to 1100 mA h g^{-1}, corresponding to *ca.* 135% of its initial value as shown in Fig. 3b.

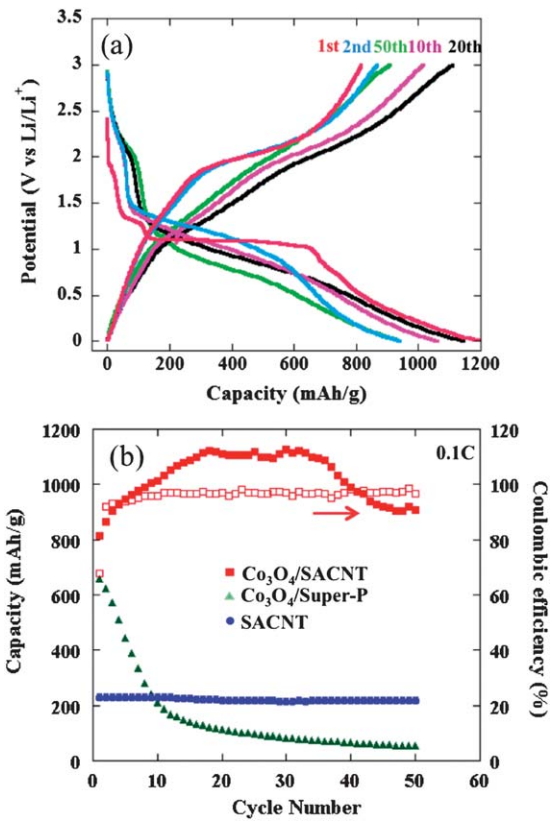

Fig. 3 (a) Galvanostatic charge–discharge curves of a 77 wt% Co_3O_4/SACNT composite at the 1st, 2nd, 10th, 20th, and 50th cycles between 3 and 0.01 V (*vs.* Li/Li^+) at 0.1 C; (b) comparison of the cycling performance of Co_3O_4/SACNT, Co_3O_4/Super-P, and SACNT films at 0.1 C, together with the Coulombic efficiency of the Co_3O_4/SACNT composite.

This phenomenon was observed for all Co_3O_4/SACNT samples. During all cycles, the Co_3O_4/SACNT composite electrode presents much better electrochemical lithium storage performance than those of Co_3O_4/Super-P and pristine SACNT electrodes. The 77 wt% Co_3O_4/SACNT composite exhibited a high reversible capacity of 910 mA h g^{-1} and a Coulombic efficiency of 97% after 50 discharge–charge cycles, based on the overall mass of the electrode. In contrast, the capacity of the Co_3O_4/Super-P electrode rapidly faded to 54 mA h g^{-1} after the same number of cycles (Fig. 3b). SACNTs displayed a stable but low capacity at 220 mA h g^{-1} in the same voltage window. Therefore, it indicates a strong synergistic effect between Co_3O_4 nanoparticles and SACNTs and its central role in the excellent cycling performance and high specific capacity of the Co_3O_4/SACNT composite.

More importantly, the Co_3O_4/SACNT electrode exhibited outstanding rate capability at a discharge rate of 0.1 C and a charge rate of 1 C (Fig. 4a). The 77 wt% Co_3O_4/SACNT composite maintained a reversible capacity of *ca.* 820 mA h g^{-1} at 1 C at initial cycles. The capacity values are calculated based on the mass of the Co_3O_4/SACNT. In comparison with literature data, this value is higher than those of Co_3O_4/graphene composites (~560 mA h g^{-1} at 0.6 C rate)[6] and Co_3O_4 nanowires (~600 mA h g^{-1} at 2.5 C rate).[20] The specific capacity at 1 C slightly decreased to *ca.* 670 mA h g^{-1} after 50 cycles. By reducing the concentration of $Co(NO_3)_2$ to 10 g L^{-1}, a composite electrode with 72 wt% of Co_3O_4 was made. The composite with a lower content of Co_3O_4 exhibited a similar initial specific capacity but a much greater capacity retention at 1 C. The specific capacity of the 72 wt% Co_3O_4/SACNT remained as high as 780 mA h g^{-1} after 50 cycles without obvious fading, which outperforms the 77 wt% Co_3O_4/SACNT composite. We therefore conclude that by changing the loading of Co_3O_4 on the SACNT film, different kinds of electrodes specifically aimed at high energy density applications, with more active materials, or high power density applications, with less active materials, can be easily fabricated. The rate performance of the 72 wt% Co_3O_4/SACNT electrode is compiled in Fig. 4b, showing specific capacities of 890 mA h g^{-1} and 720 mA h g^{-1} at 0.5 C and 2 C, respectively. The reasons for the excellent cycle stability and rate capability can be attributed to effective transport of electrons and ions that benefits from the flexible and porous SACNT framework decorated with nano-sized Co_3O_4 particles as active material.

Another significance of such Co_3O_4/SACNT composite electrodes is their high loading of active materials without additional binders and conductive agents. Compact LIBs with reduced weight can therefore be achieved. SACNTs would also act as current collectors. Accordingly, the energy density of the electrode would be greatly improved. For example, the SACNT film (100 layers) has an areal density of 0.2 mg cm^{-2}, which is only 1/80 of a commonly used 20 μm thick copper foil (16 mg cm^{-2}) in the battery industry. Furthermore, the loading of Co_3O_4 can be easily adjusted by varying the concentrations of starting materials to meet with a variety of application requirements. It could be expected that such composites composed of SACNT films and Co_3O_4 nanoparticles are a good candidate as an anode material for high-performance LIBs.

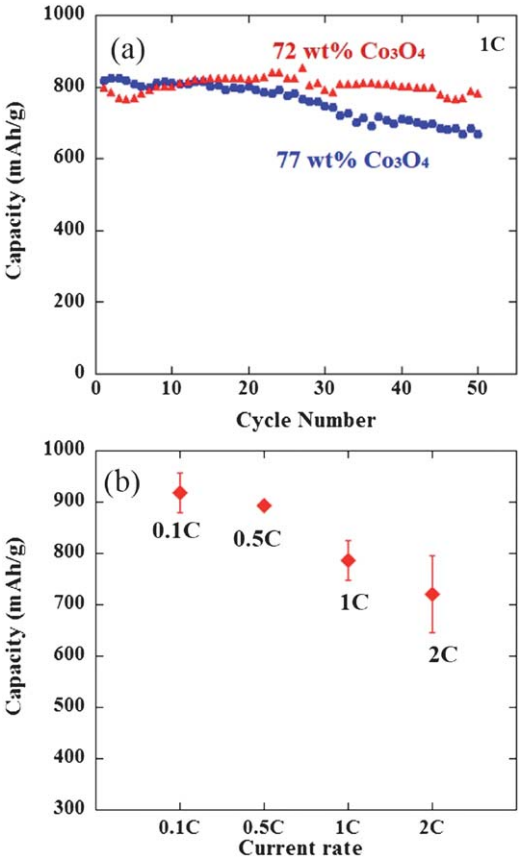

Fig. 4 (a) Comparison of the rate performance of Co_3O_4/SACNT with loading of Co_3O_4 at 72 wt% and 77 wt%; (b) rate performance of the 72 wt% Co_3O_4/SACNT composite at 0.1 C, 0.5 C, 1 C, and 2 C.

Conclusions

In summary, we have demonstrated an effective strategy to fabricate flexible Co_3O_4/SACNT composite anodes for LIBs *via* the pyrolysis of $Co(NO_3)_2$. Co_3O_4 nanoparticles with a mass loading over 70 wt% are homogeneously anchored on a flexible and highly conductive SACNT scaffold that also serves as a current collector and structural support. Effective transport of electrons and ions in the Co_3O_4/SACNT composite electrodes is achieved due to the intimate contacts of Co_3O_4 nanoparticles with the highly conductive SACNT network *via in situ* growth, nano-sized Co_3O_4 particles with shortened lithium ion diffusion length, and the porous structure of the SACNT scaffold enabling easier electrolyte infiltration and endurance in the volumetric change on cycling. The Co_3O_4/SACNT composite electrodes exhibit great cycling stability (910 mA h g^{-1} after 50 cycles at 0.1 C) as well as excellent rate performance (820 mA h g^{-1} at 1 C), based on the total mass of the electrode. Therefore, this is a promising type of anode material for high-performance LIBs. Considering the vast library of metal oxides, such a synthetic strategy could be extended to fabricate various high-performance architectures for energy storage, catalysis, sensing, photosynthesis, and other applications.

Notes and references

1 M. Armand and J. M. Tarascon, *Nature*, 2008, **451**, 652–657.
2 B. Dunn, H. Kamath and J. Tarascon, *Science*, 2011, **334**, 928–935.
3 M. M. Thackeray, C. Wolverton and E. D. Isaacs, *Energy Environ. Sci.*, 2012, **5**, 7854–7863.
4 M. Winter, J. O. Besenhard, M. E. Spahr and P. Novák, *Adv. Mater.*, 1998, **10**, 725–763.
5 P. Poizot, S. Laruelle, S. Grugeon, L. Dupont and J. M. Tarascon, *Nature*, 2000, **407**, 496–499.
6 Z. Wu, W. Ren, L. Wen, L. Gao, J. Zhao, Z. Chen, G. Zhou, F. Li and H. Cheng, *ACS Nano*, 2010, **4**, 3187–3194.
7 K. T. Nam, D. Kim, P. J. Yoo, C. Chiang, N. Meethong, P. T. Hammond, Y. Chiang and A. M. Belcher, *Science*, 2006, **312**, 885–888.
8 N. Du, H. Zhang, B. Chen, J. Wu, X. Ma, Z. Liu, Y. Zhang, D. Yang, X. Huang and J. Tu, *Adv. Mater.*, 2007, **19**, 4505–4509.
9 K. M. Shaju, F. Jiao, A. Débart and P. G. Bruce, *Phys. Chem. Chem. Phys.*, 2007, **9**, 1837–1842.
10 W. Yao, J. Wang, J. Yang and G. Du, *J. Power Sources*, 2008, **176**, 369–372.
11 A. L. M. Reddy, M. M. Shaijumon, S. R. Gowda and P. M. Ajayan, *Nano Lett.*, 2009, **9**, 1002–1006.
12 H. Wang, L. Cui, Y. Yang, H. Sanchez Casalongue, J. T. Robinson, Y. Liang, Y. Cui and H. Dai, *J. Am. Chem. Soc.*, 2010, **132**, 13978–13980.
13 Y. Wu, Y. Wei, J. Wang, K. Jiang and S. Fan, *Nano Lett.*, 2013, **13**, 818–823.
14 P. L. Taberna, S. Mitra, P. Poizot, P. Simon and J. M. Tarascon, *Nat. Mater.*, 2006, **5**, 567–573.
15 Q. Zhang, Z. Shi, Y. Deng, J. Zheng, G. Liu and G. Chen, *J. Power Sources*, 2012, **197**, 305–309.
16 M. V. Reddy, T. Yu, C. H. Sow, Z. X. Shen, C. T. Lim, G. V. Subba Rao and B. V. R. Chowdari, *Adv. Funct. Mater.*, 2007, **17**, 2792–2799.
17 B. Varghese, M. V. Reddy, Z. Yanwu, C. S. Lit, T. C. Hoong, G. V. Subba Rao, B. V. R. Chowdari, A. T. S. Wee, C. T. Lim and C. Sow, *Chem. Mater.*, 2008, **20**, 3360–3367.
18 G. Binotto, D. Larcher, A. S. Prakash, R. Herrera Urbina, M. S. Hegde and J. Tarascon, *Chem. Mater.*, 2007, **19**, 3032–3040.
19 M. Winter, J. O. Besenhard, M. E. Spahr and P. Novák, *Adv. Mater.*, 1998, **10**, 725–763.
20 Y. Li, B. Tan and Y. Wu, *Nano Lett.*, 2007, **8**, 265–270.
21 W. Zhang, X. Wu, J. Hu, Y. Guo and L. Wan, *Adv. Funct. Mater.*, 2008, **18**, 3941–3946.
22 G. X. Wang, Y. Chen, K. Konstantinov, M. Lindsay, H. K. Liu and S. X. Dou, *J. Power Sources*, 2002, **109**, 142–147.
23 D. Wang, R. Kou, D. Choi, Z. Yang, Z. Nie, J. Li, L. V. Saraf, D. Hu, J. Zhang, G. L. Graff, J. Liu, M. A. Pope and I. A. Aksay, *ACS Nano*, 2010, **4**, 1587–1595.
24 Y. Cheng, S. Lu, H. Zhang, C. V. Varanasi and J. Liu, *Nano Lett.*, 2012, **12**, 4206–4211.
25 J. Lin, Z. W. Peng, C. S. Xiang, G. D. Ruan, Z. Yan, D. Natelson and J. M. Tour, *ACS Nano*, 2013, **7**, 6001–6006.
26 S. Iijima, *Nature*, 1991, **354**, 56–58.
27 K. L. Jiang, Q. Q. Li and S. S. Fan, *Nature*, 2002, **419**, 801.
28 K. Wang, S. Luo, Y. Wu, X. F. He, F. Zhao, J. P. Wang, K. L. Jiang and S. S. Fan, *Adv. Funct. Mater.*, 2012, **23**, 846–853.
29 H. X. Zhang, C. Feng, Y. C. Zhai, K. L. Jiang, Q. Q. Li and S. S. Fan, *Adv. Mater.*, 2009, **21**, 2299–2304.
30 K. L. Jiang, J. P. Wang, Q. Q. Li, L. Liu, C. H. Liu and S. S. Fan, *Adv. Mater.*, 2011, **23**, 1154–1161.
31 K. Liu, Y. H. Sun, L. Chen, C. Feng, X. F. Feng, K. L. Jiang, Y. Y. Zhao and S. S. Fan, *Nano Lett.*, 2008, **8**, 700–705.
32 K. Liu, K. L. Jiang, Y. Wei, S. P. Ge, P. Liu and S. S. Fan, *Adv. Mater.*, 2007, **19**, 975–978.
33 X. B. Zhang, K. L. Jiang, C. Feng, P. Liu, L. N. Zhang, J. Kong, T. H. Zhang, Q. Q. Li and S. S. Fan, *Adv. Mater.*, 2006, **18**, 1505–1510.
34 D. Larcher, G. Sudant, J. Leriche, Y. Chabre and J. Tarascon, *J. Electrochem. Soc.*, 2002, **149**, A234.